UDK 546.13, 622.785

Origin of Unusual Sintering Phenomena in Compacts of Chloride-Derived 3Y-TZP Nanopowders

Sean M. Sweeney[1*)], Merrilea J. Mayo[2]
Dept. of Materials Science & Engineering, The Pennsylvania State University,
University Park, PA 16802, USA
[1] Now at GE Global Research, One Research Circle, MB-149, Niskayuna, NY 12309, USA
[2] Now at Mayo Enterprises, LLC, 12101 Sheets Farm Rd., North Potomac, MD 20878-4924, USA

Abstract:

After evaluating three alternative possibilities, the present study shows that seemingly minor amounts (at least as low as 0.06 wt%) of chlorine impurities are responsible for the poor sintering behavior observed in chloride-derived 3 mol% yttria stabilized zirconia (3Y-TZP) nanopowders. Models and quantitative estimates are used to explain the role of evolved HCl and $ZrCl_4$ gases in such anomalous behaviors as reduced sintered densities for higher green densities, de-densification, improved sintering in nitrogen over oxygen, and formation of a dense shell microstructure. Two solutions to problematic residual chlorides are compared: 1) a thermal treatment composed of an extended hold at 1000°C to allow HCl gas removal before the onset of closed porosity, and 2) a chemical treatment performed by washing bisque-fired samples at room temperature using a concentrated ammonium hydroxide solution to remove chlorides. The thermal treatment was found to be superior.
Keywords: Sintering; Zirconia; Chlorine; De-densification; Nanopowder.

1. Introduction

A variety of oxide nanopowders have been made by solution processing from chloride precursors, such as Y_2O_3 [1], TiO_2 [2], $BaTiO_3$ [3], SnO_2 [4] and doped and pure ZrO_2 [5,6]. Doped ZrO_2, in particular, has strongly documented observations of poor sinterability. Compacts of yttria-stabilized zirconia powders with crystallite sizes less than 100 nm can encounter significant sintering problems, such as an inability to reach full density under conventional heating schedules [7], cracking [8] and incomplete densification during fast firing [9], de-sintering [10] and the formation of a microstructure composed of a dense shell [11] with a significantly less dense interior. Although chlorine is known to be detrimental to the sintering of zirconia [12], the extent of the problem does not appear to be widely appreciated. In particular, the range of sintering problems that can be caused by chlorine impurities and how much chlorine can be tolerated before these sintering problems start to occur are not well known. Here, alternate mechanisms for dense shell formation during sintering are first ruled out, substantial evidence is given that residual chlorine is the root cause of dense shell formation, and the mechanisms by which residual chlorine could cause

_____
[*)] **Corresponding author**: yeneewss2000@yahoo.com

_____

this and other unusual sintering phenomena are explained. Two possible remedies to the problem of residual chlorine are then investigated, and their results compared.

2. Experimental Procedures

One nanocrystalline 3Y-TZP powder was produced by coprecipitation using zirconium dichloride oxide ($ZrOCl_2 \cdot 8H_2O$) as a precursor in a process similar to that described elsewhere [13]; the exact procedure is given in Ref. 14 [14]. This powder will hereafter be referred to as "nano 3Y-TZP". The nano 3Y-TZP powder had a BET-determined surface area (Micromeretics Gemini Model #236/00001/00, Micromeretics Instrument Corp., Norcross, GA 30093) of 58 m^2/g. Its primary particle size, as determined by x-ray diffraction (XRD) (Scintag PadV, Model #85-1852 05, Thermo ARL, Dearborn, MI 48120) line-broadening using the Sherrer equation [15] was 22 nm. For comparison, a chloride-derived, commercial 3Y-TZP powder (TZ-3Y, Tosoh Corporation, Ceramics Division, Bound Brook, NJ 08805) was used after calcination to 600º C/2h in air to remove binder, and will hereafter be referred to as "Tosoh 3Y-TZP". The properties of the nano and Tosoh 3Y-TZP powders are summarized in Tab. I.

Tab. I. The BET-determined specific surface areas and surface-area equivalent diameters, XRD line-broadening-determined crystallite sizes, and x-ray photoelectron spectroscopy (XPS) measured or manufacturer provided impurity contents for the two powders used in this study.

Powder	Specific Surface Area (m^2/g)	Surface Area-Equivalent Diam. (nm)	XRD Crystallite Diam. (nm)	Impurities (ppm)
nano 3Y-TZP	58	17	22	260 SiO_2
Tosoh 3Y-TZP	17	59	35	240 SiO_2, 220 Na_2O

To examine the effects of green density and sample size upon the sintering behavior of nano 3Y-TZP, powders were dry pressed (Carver press model C-3912, Fred S. Carver, Inc., Wabash, IN 46992-0544) in hardened steel dies, 6.4 mm (~1/4") or 10.1 mm (0.398") in diameter, with stearic acid (95 % stearic acid, Aldrich #17,536-6, Aldrich Chemical Co., Inc., Milwaukee, WI 53233) as a die-wall lubricant. Compaction pressures were 170, 440, and 1000 MPa. Green densities were calculated from geometry. The theoretical density of the solid was taken as 6.08 g/cm^3 [16]. The resultant green densities were, in order of increasing pressing pressure, 48, 53, and 58 % of theoretical.

Some larger samples (19 mm diameter, 2-3 mm thickness before drying) were made by constant rate pressure filtration of electrostatically-stabilized aqueous suspensions (pH ~3-6 achieved via nitric acid addition). For the ~5 v/o nano 3Y-TZP suspensions, urea was added at 0.25 grams per gram of water to fluidize the suspensions. Assuming no adsorption of nitric acid or urea to particle surfaces, after pressure filtration and drying there would have been ~ 0.05-0.2 wt% nitrate and ~ 4.6 wt% urea present with respect to the solid 3Y-TZP. Details of suspension preparation and pressure filtration are included in Ref. 14. Pressure filtered samples were broken by diametral compression for a study on their drying behavior, and sintering experiments were performed on the roughly half-disk samples thus obtained [14]. Pressure filtered samples, once dried, were bisque fired with little densification at 2°C/min to 500°C for 30 minutes, making them strong enough for green density measurement by the Archimedes method using water as an immersion medium. The dry green densities of

_____

pressure filtered samples of both nano and Tosoh 3Y-TZP were 55 % of theoretical.

Sintering (Carbolite bottom loading furnace model BLF 17/3, Carbolite, Inc., Watertown, WI 53094) was performed in air. Fast firing of samples was performed by introducing samples preheated to 125°C into the preheated furnace (1250°C or 1400°C) by dropping the bottom of the furnace, placing the samples directly onto an alumina plate on the furnace bottom, and raising the furnace bottom. Samples sintered for 30 minutes or less were air quenched, samples sintered for longer times were furnace cooled.

To detect possible reactions occurring during sintering, differential thermal analysis (1600 DTA, TA Instruments, a Subsidiary of Waters Co., New Castle, DE 19720) was performed on powders (ground up dried pressure filtered samples) in a platinum cup at a heating rate of 10°C/min to a temperature of 1400°C, with low surface area alumina powder as a reference.

To assess outgassing and other mass loss events, thermogravimetric analysis (TGA) (SDT2960 Simultaneous DSC-TGA, TA Instruments, a Subsidiary of Waters Co., New Castle, DE 19720) was performed. Powder samples were made by pulverizing pressure filtered samples in an alumina mortar and pestle. An alumina cup was used with heating rates of 5 and 10°C/min to 1300 or 1400°C, with subtraction of a baseline measured on the samples during cooling at 50°C/min. The temperature read by the TGA was roughly calibrated against that of the furnace used for the sintering studies by comparing densities of small samples obtained after sintering in the TGA with the densities of samples obtained from the sintering furnace. All TGA results are presented here with temperatures shifted upward by 38°C from the actual TGA temperature readings, to be approximately equivalent to the temperatures reported for the sintering furnace.

Densities of sintered samples were measured by the Archimedes technique, using water as an immersion medium. The density of water [17] was taken as 0.997 g/cm^3.

Optical microscopy of ground (800 grit) samples was performed in reflection mode at nominal magnifications of 25 to 100X. Calibrations of magnification were made with a grid of known line spacing.

Two methods were used to remove residual chlorides from the 3Y-TZP samples before the onset of closed porosity during sintering: thermal outgassing and ammonium hydroxide washing. Thermal outgassing was performed on ~2.3 mm thick pressure filtered samples by ramping at 1ºC/min and holding them at 1000°C for 10 hours in air before further sintering at higher temperatures. Ammonium hydroxide washing was performed by soaking bisque-fired (500°C/30min) ~2.3 mm thick pressure filtered samples in a 29% solution of NH_4OH in water (J.T. Baker #9721-33, Mallinckrodt Baker, Inc., Phillipsburg, NJ 08865) (~10 to 1 ratio by mass of solution to sample) for 20-24 hours, then patting dry and air drying. Ammonium hydroxide is expected to react with adsorbed HCl to form dissolved NH_4Cl and water. If all chlorine had dissolved during the soaking step, ~1% of the original chlorine should have remained after this treatment (due to the liquid trapped in the pores prior to drying).

3. Results and Discussion
3.1 Observed Densification Characteristics: Evidence Against Three Potential Origins of Poor Densification Behavior

The results of the study of Chen and Mayo [11] i.e., that thicker samples and higher heating rates generally cause lower sintered densities, were confirmed for nano 3Y-TZP samples. Fig. 1 shows that sample thickness (from 1 to 2 mm) starts to have an effect on densification behavior above a temperature of ~1050°C, for densities greater than ~75 % of theoretical.

_____

       Differences in densification behavior were also noted for different green densities, as shown for nano 3Y-TZP dry pressed samples in Fig. 2. At low temperatures, sintered density increases with increasing green density, consistent with what is normally observed in the literature [18]. At higher temperatures/longer times, sintered density decreases with increasing green density (see 1200°C/5 hr data in Fig. 2). Also, de-densification – decrease in sintered density for longer sintering times/higher temperatures – is observed in Fig. 2 for the highest green density samples. More extreme de-densification is seen in the data of Fig, 3, where the 1400°C/1h sample had a density of 79% of theoretical after having achieved at least 92% density during heating to 1400°C. As shown in Fig. 4, some samples exhibited sharp density gradients with a dense outer shell, in this case approximately 270 µm thick (~150 µm thick further into the sample) for a sample heated at 10°C/min to 1250°C/0h.
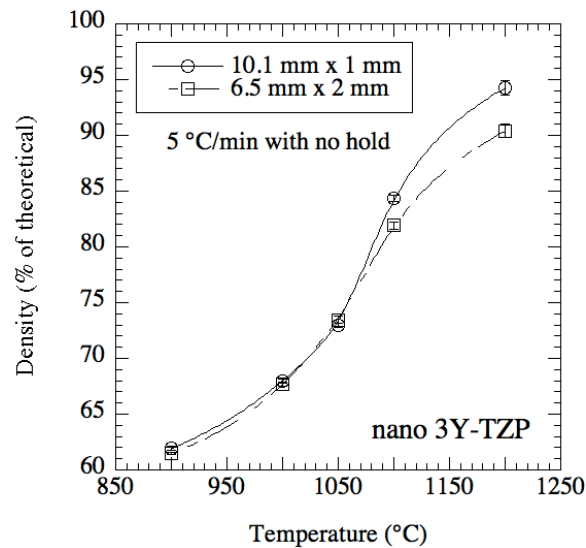

Fig. 1. Density versus temperature data from dry pressed nano 3Y-TZP disks of 58 % green
density and two different sample sizes. Curves drawn only to guide the eye.
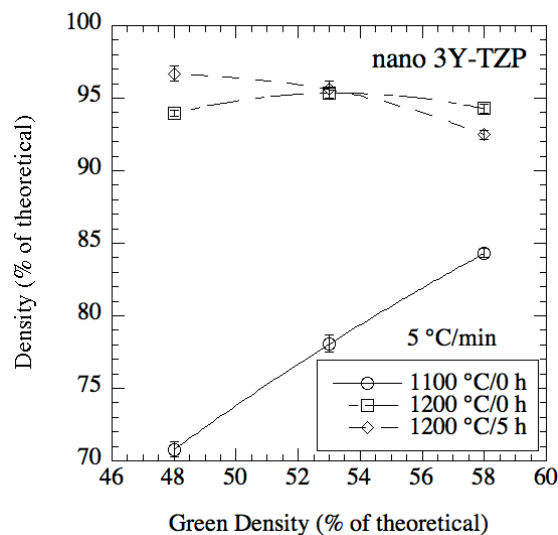
Fig. 2. Sintered density versus green density for dry pressed nano 3Y-TZP disks with initial
dimensions of 10.1 mm diameter and 1 mm thickness under various sintering schedules.
Curves drawn only to guide the eye.

_____

To determine the effect of initial particle size on the above-mentioned unusual sintering behavior, the densification response of pressure filtered Tosoh 3Y-TZP was also investigated. Sub-micron Tosoh samples suffer less than a 2 % decrease in sintered density due to fast firing effects - from 99.8 % to 98.1 % of theoretical density for heating at 5°C/min to 1400°C/1h versus fast firing to 1400°C/1h. In contrast, nano 3Y-TZP samples that sinter to 97 % of theoretical density at 1 °C/min to 1250 °C/0h reach only 85 % of theoretical density if fast fired to the same temperature with a hold of up to 1 hour. Any dense shell in the fast fired Tosoh sample could not be identified conclusively.
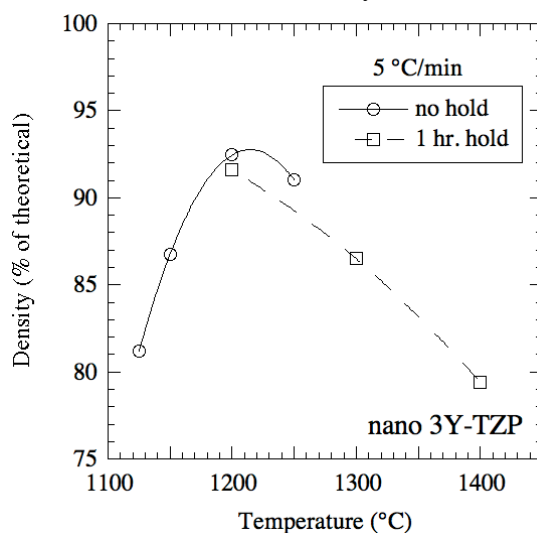
Fig. 3. Densities of ~3 mm thick nano 3Y-TZP pressure filtered samples of 55 % green density after various heating schedules show desintering.

At least four mechanisms for the formation of a density gradient from the outside to the inside of a sample during sintering have been proposed in the literature: 1) exothermic reaction with the sintering atmosphere [19] (hotter regions densify faster), 2) gradients in green density, i.e., density gradients present before sintering [20], 3) thermal gradients due to rapid heating [21,11] (in the case of zirconia, these are compounded by the low thermal conductivity of the solid [22]), and 4) evolution of a "coarsening" gas during sintering [23] "Coarsening" here refers to grain and/or pore growth without concurrent densification, a phenomenon whose linkage with hydrogen chloride gas was convincingly shown by Readey and Readey in micron-grained zirconia [24]. Chemical and particle size spatial homogeneity in the green compact have not been implicated in zirconia nanopowder sintering difficulties because of the narrow particle size distributions and homogeneous chemical compositions of powders used in most studies [7-11,20].

None of the observed heating rate, sample size, green density, and particle size dependencies of sintering are immediately inconsistent with any of the four proposed mechanisms for dense shell formation mentioned above. Nevertheless, the first mechanism – exothermic reactions - is easily eliminated by DTA experiments, which show no sudden exothermic reactions up to 1400°C for nano 3Y-TZP samples. The second mechanism – green density gradients – is eliminated by the fact that the dense shell is always observed at the exposed surface of the sample, even for pieces broken off randomly from a larger sample before sintering. Thus, the dense shell does not follow regions of maximum green density.

_____
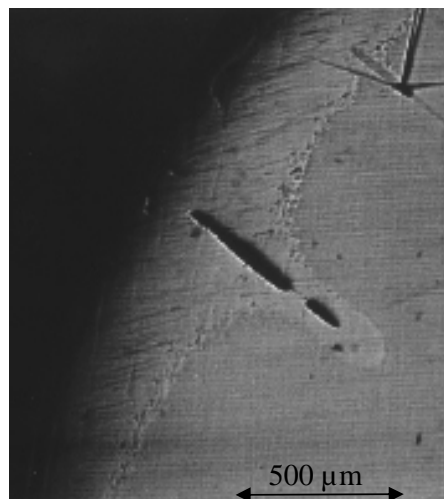
Fig. 4. Optical micrograph (reflection mode) of the cross-section of a sample of 55 % green density pressure filtered nano 3Y-TZP sintered at 10 °C/min to 1250 °C for zero time (91 % dense) showing the presence of a dense shell.

Finally, optical microscopy observations disqualify the third mechanism - thermal gradients - as the cause of the poor sintering behavior. As shown in Fig. 3, samples with severe density gradients have a dense outer shell, in this case approximately 270 µm thick (~150 µm thick further into the sample), but the "shell" also follows pre-existing internal cracks into the sample. Thus, the material that is preferentially densifying does not just follow the external sample surface as would be expected for a thermal gradient effect. Instead, the dense regions occur close to any externally-connected surface, including internal crack faces. The only way in which external heating-induced thermal gradients could form near an internal crack such that the crack surfaces could be hotter than the interior of the sample would be if the sample material had a thermal conductivity much less than air, which is not the case [22].

3.2 Observed Densification Characteristics: Evidence For Hydrogen Chloride Gas Evolution as the Cause of Poor Densification Behavior

With evidence arrayed against three potential causes of poor densification behavior, suspicion falls naturally to the fourth: evolution of structure-coarsening hydrogen chloride gas during sintering. Preferential densification near exposed surfaces, even when those surfaces are cracks running into the sample interior (Fig. 3), strongly supports a mechanism where gas migration out of the sample helps densification, and gas retention inside the sample hinders it. That the gas present contains chlorine can be seen from evidence below. Note that for pressure filtered samples, nitrates were also present due to pH adjustment of suspensions, and these nitrates could form gases at high temperatures. However, the sintering behaviors of both dry pressed (no added nitrate) and pressure filtered (with ~0.05-0.2 wt% added nitrate) samples were consistent with each other, indicating that added nitrates were not the root cause of densification issues.

X-ray fluorescence (XRF) analyses at Coorstek (Golden, CO 80403) indicated a chlorine content of about 0.20 wt% in the commercial Tosoh powder of the present study, and of about 0.18 wt% in the nano 3Y-TZP powder (these numbers are likely lower than the actual chlorine contents due to the potential loss of chlorine during the sample preparation fluxing process). For the nano 3Y-TZP powder, aqueous measurements of dissolved chloride ions with a selective ion probe (model 94-17B, Orion Research Inc, Beverly, MA 01915) after

_____

soaking a 350ºC/30min bisque fired pressure filtered part in ammonium hydroxide and then neutralizing the solution with nitric acid yielded a chlorine content of about 0.34 wt%. For Tosoh 3Y-TZP, the majority of the chlorine was not accessible to be dissolved by this method.
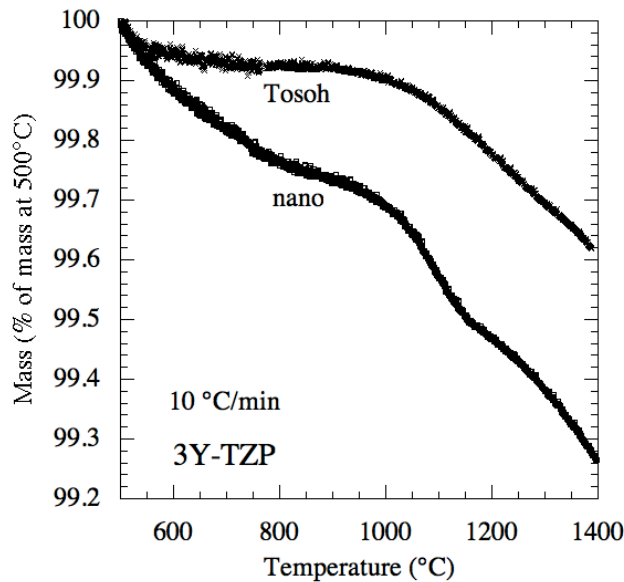
Fig. 5. TGA curves of mass versus temperature for nano and Tosoh 3Y-TZP pressure filtered samples ground into powders, and heated at 10 °C/min in flowing air.

Residual chlorine is expected to either exist as an HCl compound or react with chemisorbed water and volatize predominantly as HCl gas during sintering. TGA curves (Fig. 5) exhibit significant mass loss above ~975°C for both nano and Tosoh powders, somewhat higher than the ~700°C temperature where mass loss due to chlorine was observed to commence for another powder in the literature [25]. To estimate the mass loss due only to chlorides, a mass loss baseline curve was established by linear extension of the TGA curve from pre-875°C data. The difference between this baseline and the TGA curve at 1350°C was assumed to be due to HCl vaporization. Using this method, the measured weight losses translated into a preexisting chlorine content of 0.29 wt% for the nano powder and 0.28 wt% for the Tosoh powder, not too distant from the results of the chemical analyses for chlorine.

In the present study, evidence for a pressurized gas is observed indirectly as outward expansion of the sample walls once the pores close. At the point where pores close (1150-1200°C), the gas becomes trapped: mass loss to the outside slows significantly (~5 times slower outgassing at 1200°C than at 1100°C measured by TGA at 5°C/min heating rate on a 2 mm thick nano 3Y-TZP sample, data shown in Fig. 6. of Ref. 14). From this point onwards, the HCl gas pressure inside the still interconnected porosity in the inner part of the sample will act against the dense shell to restrict further densification of the insides of the sample. The restraining of the inner sample by the gas pressure-supported dense shell will damage the inner material as it is coarsened under both a tensile stress and a highly coarsening atmosphere. This is similar to the mechanism described by Sudre and Lange [26]. Thus a microstructure of a dense shell with a sharp interface to a significantly less dense interior with interconnected porosity may be formed. By a thin-walled pressure vessel-type effect [27], the gas pressure-induced tensile stress in the outer shell (whose thickness was observed to range from 100 to 400 µm, see Tab. II) can even be significant enough to cause macroscopic sample dimensions to progressively enlarge. This occurs by creep expansion of the outer shell with limited resistance from the damaged inner material. This outward creep is most easily

_____

detected as a decrease in sample density (de-sintering) beyond ~1200°C (Fig. 3; pores are closed above ~1175°C), and is made possible by the fact that 3Y-TZP is superplastic (creeps rapidly in response to moderate stresses) as long as its grain size is less than about a micron [28]. Calculations were performed in Ref. 14 of the amount of creep that may occur due to this thin-walled pressure vessel-type effect using the superplasticity data of Jimenez-Melendo, et al. [29]. It was determined that to account for the significant de-densification seen in Fig. 3 (from ~92 to ~79% density), one has to assume that 35 ppm of chlorine impurity evolves from the solid into the interconnected porosity of the inner sample. Only this inner gas evolution once pores close could yield high enough gas pressures to result in the requisite creep rates of the dense shell. As further evidence of this gas pressure effect, a nano 3Y-TZP part was sintered at 5°C/min to 1200°C/1h and achieved a density of 90.3%, then a section of its dense shell region was cut away, exposing the interconnected porosity of the inner material; after re-sintering at 5°C/min to 1300°C/1h, this part actually densified somewhat to 94.1% rather than undergoing de-densification as had been observed in previous sintering runs where the dense shell had been left intact (and as evidenced in Fig. 3).

Tab. II. Thicknesses of dense shells measured upon 55% green density pressure filtered nano 3Y-TZP samples, ~3 mm thick, sintered at various heating rates to 1250°C/0 min.

| Heating Rate (°C/min)	Approximate Dense Shell Thickness (μm)	Density of Sintered Sample (%)
10	110-170	90
5	120-160	91
2.5	320-400	93
1	>1500 (entire sample)	97

A significant chlorine content in the samples, gaseous emission (mass loss) on heating, more complete densification near exposed surfaces (i.e., wherever coarsening gas can escape, and air can diffuse in to lessen the coarsening effect of the gas, see below), and an outward creep of sample walls all support the hydrogen chloride coarsening gas hypothesis over other hypotheses. All other densification problems are at least consistent with the hydrogen chloride gas hypothesis. A slower heating rate allows more time for gas to escape before closed porosity forms, and hence results in higher density samples. Thinner samples yield higher densities because more of the sample is close to an external surface where the partial pressure of coarsening gas in the pores is lower, and thus densification is less hindered. Finer powders experience more severe sintering problems because they densify faster [30], thus lowering the onset temperature for closed porosity, to temperatures where outgassing is not complete. Smaller particles also result in lower permeabilities, thus hindering the escape of gases from samples (note: the ratio of the permeabilities to liquid determined by pressure filtration on wet bodies of Tosoh 3Y-TZP and nano 3Y-TZP was nearly 15). Thus, gradients in sintered density - including dense shells - are more likely to form during heating with evolution of HCl gas. Lower permeabilities and lower onset temperatures for closed porosity are also characteristic of high green density samples, which explains why greater green densities do not consistently yield greater sintered densities for nano 3Y-TZP samples.

3.3 Quantitative Estimate of Chloride Effects in Sintering of 3Y-TZP

The experiments of Readey and Readey [24] in which powder compacts of sub-micron undoped zirconia were intentionally sintered in 1 atm of HCl have previously demonstrated substantial pore and grain coarsening, as well as the poor densification that can result from HCl-rich environments. The dominant reaction by which HCl causes effective volatilization of zirconia and thus allows microstructural coarsening by vapor phase transfer

_____

of matter is:

$$ZrO_2(s) + 4HCl(g) = ZrCl_4(g) + 2H_2O(g) \qquad (1)$$
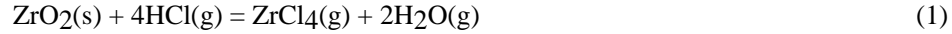
The partial pressure of $ZrCl_4$ is strongly dependent upon the relative partial pressures of air (specifically oxygen and water vapor) and HCl gas.

The finite difference method was applied to the dusty gas model [31] to find the partial pressure distributions of air and of HCl gas in the pores of the solid. Details of these calculations are given in Ref. 14. To sufficient first approximation, assuming zero partial pressure of HCl at the sample surface (i.e., assuming that diffusion/flow of the HCl gas away from the sample surface was much faster than flow through the sample pores), the partial pressure distributions of air and HCl in the pores of an infinite slab of thickness 2L with a constant mass rate of gas production per unit sample volume, g_g, are given by

$$P_{HCl} \approx \frac{g_g RT L^2}{2 W_{m,HCl} D_{K,HCl}} \left(-(x/L)^2 + 1\right) \qquad (2)$$

$$P_{air} \approx \left(\frac{k_l P_{surf}/\eta_{air}}{D_{K,air} + k_l P_{surf}/\eta_{air}}\right)\left(\frac{g_g RT L^2}{2 W_{m,HCl} D_{K,HCl}}\right)\left(-(x/L)^2 + 1\right) + P_{surf} \qquad (3)$$

where $D_{K,HCl}$ and $D_{K,air}$ are the Knudsen diffusion coefficients of HCl and air, respectively, P_{surf} is the gas pressure at the sample surface (taken as 101325 Pa, i.e., 1 atm), R is the ideal gas constant, T is absolute temperature, x is a coordinate ranging from -L at one sample surface to L at the other sample surface, η_{air} is the viscosity of air, k_l is the permeability to liquid, and $W_{m,HCl}$ is the molecular weight of HCl (36.45 g/mol). It was assumed that the viscosities of HCl and air are the same (5×10^{-5} Pa-s [32]), and do not change significantly with temperature/pressure. The Knudsen diffusion coefficient of air can be determined from [31,33]

$$D_{K,air} = \frac{k_l^{0.67}}{\eta_{air}} \left(\frac{T}{298.15}\right)^{0.5} \qquad (4)$$

The Knudsen diffusion coefficient of HCl was estimated from [34]

$$D_{K,HCl} = D_{K,air}\left(W_{m,air}/W_{m,HCl}\right)^{1/2} \qquad (5)$$

where $W_{m,air}$ and $W_{m,HCl}$ are the molecular weights of air and HCl, respectively.

The permeability to liquid was assumed to vary linearly with density from the value estimated [14] for the dry green state from permeability measurements during pressure filtration, to a value of zero at 90% of theoretical density:

$$k_l = 7.714 x 10^{-19} - 8.571 x 10^{-19} \rho \qquad (6)$$

This form of approximate permeability dependence upon density is apparent in the gas permeability data of Glass and Green [35].

The gas evolution rate was chosen so that the calculated mass loss due to HCl flow through the sample surface matched the nearly constant (from 1000°C to 1125°C) rate of mass loss (70 µg/g/min) occurring during a TGA run on a 2.04 mm thick nano 3Y-TZP sample heated at 5°C/min. Fig. 6 shows the results of the finite difference calculations for the total gas pressure and HCl gas partial pressure versus depth into the sample for a pressure filtered nano 3Y-TZP sample at a temperature of 1100°C, and a density of 75 % of theoretical. The program Factsage[TM] (GTT- Technologies, 52134 Herzogenrath, Germany) was used to determine the equilibrium $ZrCl_4$ partial pressures shown in Fig. 7 based upon the HCl and air partial pressures (Equilib-Web was also used for some supplemental calculations: http://www.crct.polymtl.ca/equiweb.php). Air was assumed to be 80% N_2, 20% O_2, i.e., it was assumed to be perfectly dry. The presence of water vapor in the air in the pores will further lower the $ZrCl_4$ partial pressures from what is reported here, but generally by not more than a factor of 2 near the sample surface (less so inside the sample where the mole fraction of air is

_____

lower) for 1 mol% of water in the air (corresponding to a relative humidity of 37 % at 23 °C). As Fig. 7 shows below, this factor of 2 would not cause a major change in the predicted dense shell thickness due to the rapid drop-off in $ZrCl_4$ partial pressures near the sample surfaces. The effect of relative humidity of the lab air on sintering behavior and dense shell thickness was not studied.
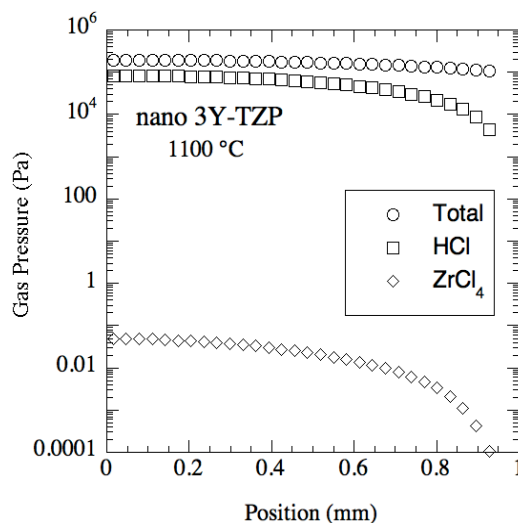
Fig. 6. Calculated total gas pressure and partial pressures of HCl and $ZrCl_4$ versus position (zero is the sample center; the sample surface is at 0.943 mm) in a ~2 mm thick pressure filtered nano 3Y-TZP sample at 1100°C (relative density = 0.75) undergoing heating at 5°C/min.

To estimate the vapor pressures of $ZrCl_4$ necessary for evaporation/condensation coarsening to play a significant role in the sintering behavior of 3Y-TZP, the equations of Swinkels and Ashby [36] were used to calculate relative neck growth rates due to densification and due to vapor phase transport. This was done for minimum and most probable gas-coarsened neck sizes; details of these calculations are available upon request and are essentially given elsewhere [14], with one noTab. change being that most probable gas-coarsened neck diameter is taken here as 85% of the grain diameter (supported by the data of Readey et al. [24]), not 98% as in Ref. 14. Grain sizes were either measured by x-ray line broadening or estimated at different points in heating by using grain size data from Refs. 11 and 38 to construct a master grain size curve [37] for the material, with the furnace temperature in the present study roughly calibrated by comparing densities and grain sizes to those reported in Refs. 11 and 38 to be 50ºC hotter, i.e., a reported temperature of 1050ºC in Ref. 10 corresponds to a temperature of 1100ºC in this study [38]. From Fig. 7 for nano 3Y-TZP (grain size of 46 nm determined by XRD line broadening), it is apparent that the rate of neck growth due to evaporation/condensation calculated using the partial pressures of $ZrCl_4$ shown in Fig. 6 is equal to the calculated rate of neck growth due to grain boundary diffusion in the range from about 60 to 200 μm into the sample (corresponding to partial pressures of $ZrCl_4$ of between approximately 7.0×10^{-4} Pa and 6.2×10^{-3} Pa (6.9×10^{-9} atm and 6.1×10^{-8} atm)). This 60 to 200 μm depth into the sample agrees well with the measured dense shell thickness, which was 120 to 160 μm for a pressure filtered nano 3Y-TZP sample heated at 5°C/min to 1250°C/0 min. In this work it was assumed that residual chlorine would evolve as HCl, which seems likely since the 3Y-TZP was made by a chemical co-precipitation process in water. If the residual chlorine were instead assumed to evolve as Cl_2 and 1% water vapor was assumed to be in the air during sintering, then the predicted dense shell thickness range would be ~20

_____

to ~35 μm, i.e., significantly lower than observed. Although a density of 75% of theoretical and a temperature of 1100ºC were used in these calculations, calculations at other densities/temperatures show that the predicted dense shell thickness when assuming a fixed ratio of neck radius to particle radius of 0.85 does not vary by more than about 20% until a density of ~85% of theoretical is achieved, at which point the predicted thickness decreases. When assuming the minimum geometrically-determined neck radius, the dense shell thickness decreases with density/temperature, for instance by a factor of about 3 when going from a density of 60% to 80%, and temperatures from 1000ºC to 1120ºC. Clearly this is a simplified model that makes many assumptions about the exact gas composition and the geometry of the sintering model, but it appears to be sufficient to predict approximate dense shell thicknesses for nano 3Y-TZP samples.
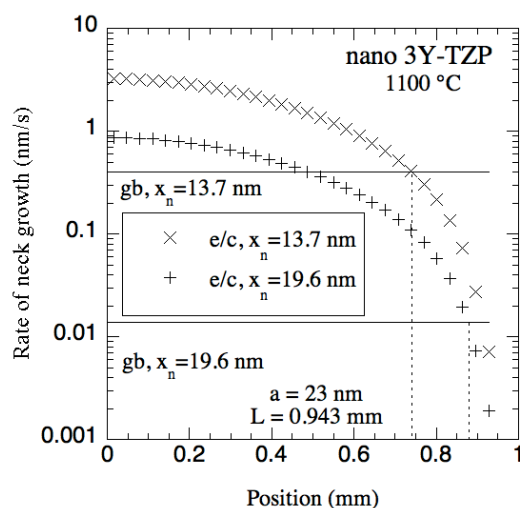
Fig. 7. The rate of neck growth at 1100°C due to grain boundary (gb) diffusion and evaporation/condensation (e/c) versus position in a pressure filtered nano 3Y-TZP sample sintering at a constant heating rate of 5°C/min. Two extremes (small and large) of the neck radius (x_n) were used for calculating the curves.

Similar calculations show that, for pressure filtered Tosoh 3Y-TZP samples heated at 5°C/min (mass loss rate of 40 μg/g/min) at 1200°C, a density of 71% of theoretical, and an estimated grain size of 91 nm, grain boundary diffusion dominates over evaporation/condensation coarsening throughout the sample thickness, consistent with the lack of dense shell formation in these samples. It should be noted that from these calculations, the predicted sample thickness at which a dense shell would form in Tosoh 3Y-TZP heating at 5°C/min would be ~3 to 4 mm (depending on the assumed neck to grain size ratio). In a study by Seidensticker and Mayo [39], densities of >98% were observed when sintering Tosoh 3Y-TZP samples of final dimensions of 9.4 mm diameter and 14.5 mm height at 5°C/min to 1350ºC/1h. They did not report observation of a dense shell type microstructure, but their obtained density range of greater than 98% rather than 99% of theoretical is similar to the 98% density seen in the current study for fast firing of ~3 mm thick Tosoh 3Y-TZP to 1400ºC/1h. In a study on fast firing of chlorine-containing yttria-stabilized zirconias by Kim and Kim, samples started out 10-15 mm in diameter and 5-7 mm in thickness [9,40]. For Tosoh 3Y-TZP, they observed a decrease in final density from 99.3% to 95.8% to 90.7% of theoretical when the heating rate to 1430ºC/1h was changed from 10ºC/min to 50ºC/min to 500ºC/min, respectively. They did not report any microstructures or indicate that a dense shell had been observed.

_____

Thus it seems that density gradients in Tosoh 3Y-TZP are generally less severe than for nano 3Y-TZP and that the onset of these density gradients may come under somewhat more severe thickness and heating rate conditions than predicted by a simplified model of a crossover in neck growth mechanism. Both Guillon, et al. [41] and Garino and Bowen [42] found that for constrained sintering of a thin film of alumina on a rigid substrate, the densification rate was less than that for a free body of alumina. It seems reasonable to assume a similar effect for 3Y-TZP. In the current scenario, the outer shell region attempts to densify at early sintering stages while constrained by the less quickly densifying inner material. If the ability to densify while being constrained decreases with increasing grain and/or pore size, this could explain some of the differences between the nano and Tosoh 3Y-TZP densification/density gradient formation behaviors. This may be expected due to both the higher sintering stresses and creep rates during dense shell formation that would be present in the nano 3Y-TZP than in the Tosoh 3Y-TZP. Another factor could be that since the temperature at which significant closed porosity starts to form for Tosoh 3Y-TZP is approximately 115ºC higher than for nano 3Y-TZP, the escape of HCl before closed porosity forms, and the rate of diffusion of HCl through the dense shell and out of the Tosoh 3Y-TZP sample will likely be higher. This means that less gas will be truly trapped or continue to evolve in pores after dense shell formation, thus limiting the gas pressure that would constrain further densification or contribute to desintering.

3.4 Comparison of Methods to Alleviate Chloride Gas-Induced Sintering Problems

Two methods were used to remove residual chlorides from nano 3Y-TZP samples before the onset of closed porosity during sintering. As described in the Experimental Procedure, the first was a thermal outgassing treatment at 1000°C/10 hr. The second was a chemical washing treatment in which bisque-fired samples were soaked in a 29 % solution of NH_4OH. This soaking resulted in 33% of the original chlorine remaining (by XRF), not the 1% predicted if all the chlorine had dissolved into the NH_4OH solution, likely indicating that all the chlorine was not on particle surfaces. The effect of the chloride removal treatments on sample density achieved after sintering at 5°C/min to 1200°C/1 hr is shown in Fig. 8 (with chlorine contents determined by XRF). Density is seen to increase with decreasing chlorine content: the highest chlorine content and lowest density occur in the sample as-is, and the lowest chlorine content and highest density occur in the sample heat treated to 1000°C/10 hr. Dense shells were not observed in either of the samples that had undergone chloride removal treatments; dense shells could not readily be observed by a fine grind and optical microscopy method above about 93% density for any of the samples in this study. The thermal pre-treatment of one sample, after which the density was measured as 73.2%, enabled a final density of 99.0% to be achieved after fast firing the same sample to 1200ºC/1h. This is significantly higher than the 85-86% density achieved with similar samples fast fired to 1200ºC/1h with no thermal pre-treatment.

The line fitted to the data in Fig. 8 is drawn to arbitrarily pass through 100% density at zero chlorine content. It should be noted that this plot is only valid for this particular powder, green density, sample size, and heating rate. Nonetheless, in the sintering of nanocrystalline 3Y-TZP, it is clear that chlorine contents at least as low as 0.06 wt% (600 ppm) can cause significant problems in achieving full density under conventional pressureless sintering conditions in air. Saito and Ikegami [43] studied the effect of chlorine on sintering of yttria-stabilized zirconia and found that as little as 0.01 wt% of chlorine resulted in a significantly lower density for treated Tosoh 3Y-TZP samples sintered under vacuum compared to samples with <50 ppm Cl present (87% versus 99.9% density, respectively). Under sintering in air, however, up to 0.05 wt% Cl lowered sintered densities by less than 1%.

_____
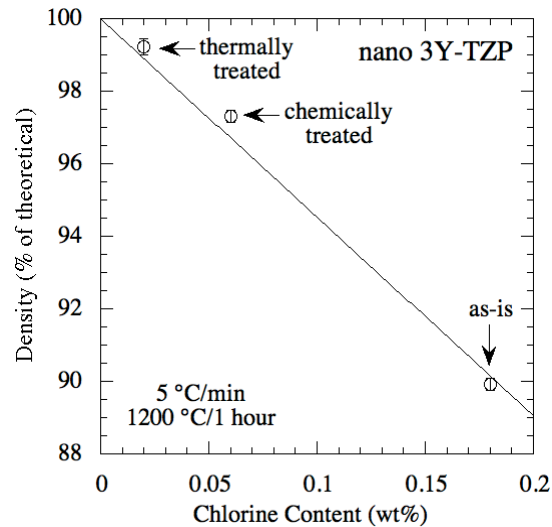
Fig. 8. The density achieved after sintering at 5°C/min to 1200°C/1hr varies considerably with the chlorine content for 2.3 mm thick pressure filtered nano 3Y-TZP samples of 55 % green density.

4. Application to Other Studies

The mechanism of dense shell formation/desintering discussed here may be at least partly responsible for the sample bloating [10,44] (reported in Ref. 10 as associated with carbon evolution as CO_2, and in Ref. 44 as due to oxygen evolution during transformation to cubic zirconia at high temperature), de-densification [45] (reportedly due to a chlorine impurity), more dense exterior and less dense interior [20,46] (reportedly due to gradients in green density), distinct dense shell microstructure [11] (reportedly due to thermal gradients), poorer sintering behavior in oxygen than in nitrogen [47] (reportedly associated with nitrogen solubility in zirconia), and cracking at high heating rates [8] (no explanation given) found in the literature on sintering of yttria-doped zirconia powders. Note that the reportedly poorer sintering behavior in oxygen than in nitrogen could be due to a more uniform coarsening of the microstructure (less of a dense shell) in nitrogen than in oxygen owing to nitrogen not preferentially suppressing $ZrCl_4$ partial pressures in the outer region of the sample compared to oxygen. More uniform coarsening could enable more gas escape from the sample before significant closed porosity forms, thus avoiding later densification inhibition due to entrapped gas. The thermal evolution of HCl gas may also play some role in the success of two-step sintering of 3Y-TZP [48].

The results of Lanin et al. [49] for the sintering of zirconium carbide showing dense shell formation (originally explained to be due to thermal gradients) during fast firing are also likely explained by a coarsening gas mechanism. The residual oxygen (0.33 wt%) and free carbon (0.04 wt%) in their system are likely to react during sintering to form CO(g) and ZrO(g), providing vapor phases which can coarsen the zirconium carbide microstructure. This is similar to the explanation proposed by Ness and Rafaniello [23] for the formation of density gradients in silicon carbide samples.

_____

5. Conclusions

Four possibilities for the poor densification behavior of chloride-derived 3Y-TZP nanopowders were examined: (1) exothermic reaction with the sintering atmosphere, (2) gradients in green density, (3) thermal gradients due to rapid heating, and (4) evolution of a structure-coarsening chloride gas during sintering. Densification experiments and thermal analysis show the evolution of structure-coarsening hydrogen chloride gas to be the only consistent explanation across all observed phenomena, including no sharp exothermic peaks in a DTA scan (ruling out the first possibility), dense shell formation always along exposed surfaces of randomly fractured samples (ruling out the second possibility), dense shell formation along pre-existing cracks (ruling out the third possibility), mass loss at high temperature in a TGA scan (supporting the fourth possibility), de-densification by outward creep of the dense shell (as a result of a thin-wall pressure vessel effect when pores close in the dense shell region and gas is trapped in the interior of the sample), improved densification (with no detecTab. dense shell) when either a chemical wash step or an intermediate thermal treatment was added to remove residual chlorides before final sintering, and higher heating rates, higher green densities, and larger sample sizes all exacerbating densification issues due to less time/greater resistance for gas to escape before closed porosity forms.

To determine the crossover from grain boundary diffusion densifying to evaporation/condensation-type coarsening mechanisms in a sintering sample, finite difference calculations were performed using the dusty gas model [31]. The air and HCl partial gas pressure distributions were determined within samples, then thermodynamic calculations were performed to determine $ZrCl_4$ partial pressure distributions, and finally neck growth rate calculations were performed using the sintering model of Swinkels and Ashby [36]. For a nano 3Y-TZP sample heated at 5°C/min, the calculated transition between grain boundary diffusion-dominated (densifying) neck growth and evaporation/condensation-dominated (coarsening) neck growth occurs at a depth into the sample that agrees well with the observed dense shell thickness of 120-160 μm. These gas evolution, thermodynamic, and sintering calculations also point to the difference in sintering behaviors between nano and Tosoh 3Y-TZP powder compacts as likely stemming first from the factor of approximately 15 difference in permeability between the two sample types owing to differences in initial particle size, second from the ~115ºC difference in pore closure temperature making entrapment of significant residual chlorine in nano 3Y-TZP samples more likely, and third possibly from a difference in relative amounts of constraint by the inner material of the outer sample shell from densifying owing to grain and pore size differences between the samples.

The problems related to a structure-coarsening gas can be minimized by allowing the gas to evolve at a temperature below that at which significant closed porosity forms and/or by washing partially sintered (bisque-fired) samples to remove the gas-former. A nano 3Y-TZP sample washed with an NH_4OH solution still had a residual chlorine content of 0.06 wt%, though, enough to show inhibited densification relative to a thermally treated sample with a residual chlorine content of 0.02 wt%.

_____

6. References

1. P.K. Sharma, M.H. Jilavi, R. Nab, H. Schmidt, *J. Mat. Sci. Lett.*, 17 (1998) 823-5.
2. Y. Zhu, L. Zhang, C. Gao, L. Cao, *J. Mat. Sci.*, 35 (2000) 4049-54.
3. H. Xu, L. Gao, *J. Am. Ceram. Soc.*, 86 (2003) 203-5.
4. M. Epifani, M. Alvisi, L. Mirenghi, G. Leo, P. Siciliano, L. Vasanelli, *J. Am. Ceram. Soc.*, 84 (2001) 48-54.
5. A.J.A. Winnubst, G.S.A.M. Theunissen, M.M.R. Boutz, A.J. Burggraaf, in: "Structural Ceramics Processing, Microstructure, and Properties," Eds. J.J. Bentzen, J.B. Bilde-Sorensen, N. Christiansen, A. Horsewell, and B. Ralph, Riso National Laboratory, Roskilde, Denmark, 1990, p. 523-8.
6. C. Feng, H. Qui, J. Guo, D. Yan, W.A. Schulze, *J. Mat. Synth. Proc.*, 3 [1] (1995) 25-9.
7. R. Oberacker, K. Dorfschmidt, T. Liu, F. Thummler, in: "Science of Sintering: New Directions for Materials Processing and Microstructural Control," Eds. D.P. Uskokovic, H. Palmour, III, and R.M. Sprigs, Plenum Press, New York, 1989, p. 357-66.
8. J. Wilson, S.M. Kunz, *J. Am. Ceram. Soc.*, 71 (1988) C40-C41.
9. D.-H. Kim, C.H. Kim, *J. Am. Ceram. Soc.*, 75 (1992) 716-8.
10. P. Kountouros, H. Schubert, in: "Euro-Ceramics II, v.2 Structural Ceramics and Composites," Eds. G. Ziegler and H. Hausner, Deutsche Keramische Gesellschaft e.V., Koln, Germany, 1991, p. 775-9.
11. D.-J. Chen, M.J. Mayo, *J. Am. Ceram. Soc.*, 79 (1996) 906-12.
12. C.E. Scott, J.S. Reed, *Am. Ceram. Soc. Bull.*, 58 [6] (1979) 587-90.
13. M. Ciftcioglu, M.J. Mayo, in: "Superplasticity in Metals, Ceramics, and Intermetallics," Eds. M.J. Mayo, M. Kobayashi, and J. Wadsworth, MRS, Pittsburgh, 1990, p. 77-87.
14. S.M. Sweeney, S.M., *Permeability, Drying, and Sintering of Pressure Filtered Ceramic Nanopowders*, PhD Thesis, The Pennsylvania State University, University Park, PA, 2005.
15. R. Jenkins, R.L. Snyder, *Introduction to X-ray Powder Diffractometry*, John Wiley & Sons, Inc., New York, 1996, p. 89-90.
16. R.P. Ingel, D. Lewis, III, *J. Am. Ceram. Soc.*, 69 (1986) 325-32.
17. D.R. Lide, *CRC Handbook of Chemistry and Physics*, 72nd ed., CRC Press, Inc., Boca Raton, FL, 1991, p. 6/9.
18. J. White, in: "Sintering and Related Phenomena," Eds. G.C. Kuczynski, N.A. Hooton, and G.F. Gibson, Gordon & Breach, New York, 1967, p. 245-69.
19. E. Suvaci, G. Simkovich, G.L. Messing, *J. Am. Ceram. Soc.*, 83 (2000) 1845-52.
20. H. Schubert, P.W. Kountouros, J. Pross, G. Petzow, A.O. Boschi, in: "Science and Technology of Zirconia V," Eds. S.P.S. Badwal, M.J. Bannister, and R.H.J. Hannink, Technomic Publishing Co., Inc., Lancaster, PA, 1993, p. 292-8.
21. D.E. Garcia, J. Seidel, R. Janssen, N. Claussen, *J. Eur. Ceram. Soc.*, 15 (1995) 935-8.
22. S. Raghavan, H. Wang, R.B. Dinwiddie, W.D. Porter, M.J. Mayo, *Script. Mat.*, 39 (1998) 1119-25.
23. E.A. Ness, W. Rafaniello, *J. Am. Ceram. Soc.*, 77 (1994) 2879-84.
24. M.J. Readey, D.W. Readey, *J. Am. Ceram. Soc.*, 69 (1986) 580-2.
25. C.E. Scott, J.S. Reed, *Bull. Am. Ceram. Soc.*, 58 [6] (1979) 587-90.
26. O. Sudre, F.F. Lange, *J. Am. Ceram. Soc.*, 75 (1992) 3241-51.
27. R.C. Hibbeler, *Mechanics of Materials*, Macmillan Publishing Co., New York, 1991, p. 373-4.

28. T.G. Nieh, J. Wadsworth, *Acta Metall.*, 38 (1990) 1121-1133.
29. M. Jimenez-Melendo, A. Dominguez-Rodriguez, A. Bravo-Leon, *J. Am. Ceram. Soc.*, 81 [11] (1998) 2761-76.
30. C. Herring, *J. Appl. Phys.*, 21 (1950) 301-3.
31. S.W. Webb, K. Pruess, *Transport in Porous Media*, 51 (2003) 327-41.
32. K. Kadoya, N. Matsunaga, A. Nagashima, *J. Phys. Chem. Ref. Data*, 14 (1985) 947-70.
33. D.C. Thorstenson, D.W. Pollock, *Water Resour. Res.*, 25 (1989) 477-507.
34. S.W. Webb, *J. Porous Media*, 1 (1998) 187-99.
35. S.J. Glass, D.J. Green, *J. Am. Ceram. Soc.*, 82 (1999) 2745-52.
36. F.B. Swinkels, M.F. Ashby, *Acta Metall.*, 29 (1981) 259-81.
37. H. Su, D.L. Johnson, *J. Am. Ceram. Soc.*, 79 [12] (1996) 3211-17.
38. D.-J. Chen, *Densification and Microstructural Evolution in Nanocrystalline Yttria-Stabilized Zirconia Ceramics*, Masters Thesis, The Pennsylvania State University, 1994.
39. J.R. Seidensticker, M.J. Mayo, *Scripta Materialia*, 38 [7] (1998) 1091-1100.
40. Personal communication from D.-H. Kim, 2012.
41. *O. Guillon, E. Aulbach, J. Rodel, R.K. Bordia,* J. Am. Ceram. Soc*., 90 [6] (2007) 1733-7.*
42. T.J. Garino, H.K. Bowen, *J. Am. Ceram. Soc.*, 73 [2] (1990) 251-7.
43. N. Saito, T. Ikegami, *J. Ceram. Soc. Japan*, 109 [9] (2001) 738-41.
44. F.F. Lange, H. Shubert, N. Claussen, M. Ruhle, *J. Mat. Sci.*, 21 (1986) 768-74.
45. A.V. Galakhov, S.V. Kutsev, V.A. Kryuchkov, A.V. Prokof'ev, I.A. Litvinov, *Refractories*, 34 [1-2] (1993) 70-81.
46. W. Li, L. Gao, *J. Eur. Ceram. Soc.*, 20 (2000) 2441-5.
47. Y.-K. Paek, J.-H. Ahn, G.-H. Kim, S.-J.L. Kang, *J. Am. Ceram. Soc.*, 85 (2002) 1631-33.
48. M. Mazaheri, A. Simchi, F. Golestani-Fard, *J. Eur. Ceram. Soc.*, 28 [15] (2008) 2933-9.
49. A.G. Lanin, E.V. Marchev, S.A. Pritchin, *Ceram. Int.*, 17 (1991) 301-7.

Садржај: *Након евалуације три алтернативне могућности, рад указује на то да је наизглед мала количина нечистоће (мање од 0,06 тежинских% хлора) одговорна за недовољно синтеровање нано-праха (3Y-TZP). Употребљени су модели и квантитативна предвиђања да би објаснила улогу гаса HCl и ZrCl₄ за такве аномалије приликом синтеровања, као што су смањење густине након синтеровања, побољшано синтеровање у азоту од синтеровања у ваздуху и формирање густе шкољкасте микроструктуре. Две солуције за решавање проблематике су упоређиване: 1) термички третман који се сатојао од задржавања на 1000°C да се дозволи гасу HCl да испари пре затварања пора, и 2) хемијски третман који се сатојао у испирању узорака на собној температури употребом концентрованог амонијум хидроксида да би се уклонио хлор. Термички третман је дао боље резултате.*
Кључне речи: *синтеровање, хлор, слаба денсификација, нано-прах.*